

Microbiome subcommunity learning with logistic-tree normal latent Dirichlet allocation

Patrick LeBlanc

Department of Statistical Sciences, Duke University
and

Li Ma*

Department of Statistical Sciences, Duke University

May 17, 2022

Abstract

Mixed-membership (MM) models such as Latent Dirichlet Allocation (LDA) have been applied to microbiome compositional data to identify latent subcommunities of microbial species. However, microbiome compositional data, especially those collected from the gut, typically display substantial cross-sample heterogeneities in the subcommunity composition which current MM methods do not account for. To address this limitation, we incorporate the logistic-tree normal (LTN) model — using the phylogenetic tree structure — into the LDA model to form a new MM model. This model allows variation in the composition of each subcommunity around some “centroid” composition. Incorporation of auxiliary Pólya-Gamma variables enables a computationally efficient collapsed blocked Gibbs sampler to carry out Bayesian inference under this model. We compare the new model and LDA and show that in the presence of large cross-sample heterogeneity, under the LDA the resulting inference can be extremely sensitive to the specification of the total number of subcommunities as it does not account for cross-sample heterogeneity. As such, the popular strategy in other applications of MM models of overspecifying the number of subcommunities—and hoping that some meaningful subcommunities will emerge among artificial ones—can lead to highly misleading conclusions in the microbiome context. In contrast, by accounting for such heterogeneity, our MM model restores the robustness of the inference in the specification of the number of subcommunities and again allows meaningful subcommunities to be identified under this strategy.

Keywords: Microbiome, mixed-Membership models, latent variable models, compositional data, Bayesian inference

*Email: li.ma@duke.edu

1 Introduction

The human gut microbiome is the genetic content of all bacteria, archaea, viruses, and eukaryotic microbes residing in the human gut and it is commonly used to profile the composition of the gut microbiota, the set of all such microbes. Advances in next-generation sequencing techniques have substantially reduced the cost of this approach and made it widely accessible. One highly cost-effective microbiome profiling strategy is based on targeting a single marker gene, typically the 16S ribosomal RNA (rRNA) gene, through amplicon-based sequencing [Li \[2015\]](#). A more expensive, but more precise, approach is whole-genome shotgun metagenomic sequencing [Beghini et al. \[2021\]](#). Traditionally the sequencing reads have been clustered into Operational Taxonomic Units (OTUs), which serve as the basic unit of microbial taxa. Recently, amplicon sequencing variants (ASVs) have come into a wider use as they can achieve more precise characterization of microbial species and resolve the sample-specificity issue of the OTU [Callahan et al. \[2017\]](#). Our work is applicable to either method of characterizing microbial taxa; in the following we shall generically refer to the basic unit as ASVs.

Gut microbiome studies often involve highly heterogeneous samples due to the multitude of factors that can influence an individual’s gut microbiota. A useful analytical method for analyzing microbiome compositions is thus to classify microbiome samples into clusters characterized by a particular compositional signature. In the context of gut microbiome, these clusters are called “enterotypes” [Costea et al. \[2018\]](#) and they have been found to be associated with various health outcomes [Del Chierico et al. \[2014\]](#). A number of microbiome clustering methods have been introduced in recent years. One of the simplest and most popular methods is the Dirichlet-multinomial mixture (DMM) model [Holmes et al. \[2012\]](#), [Nigam et al. \[2000\]](#), which uses a hierarchical structure to allow within-cluster sample-to-sample variability in the microbial compositions. However, the DMM is too restrictive to realistically characterize the within-cluster, cross-sample variance present in microbiome data [Tang et al. \[2018\]](#), [Wang and Zhao \[2017\]](#) as it uses a single concentration parameter to characterize the covariance structure across the microbial taxa. More general methods have recently been introduced to resolve this limitation [Mao et al. \[2020\]](#), [Tang et al. \[2018\]](#).

Such clustering analysis, however, makes the implicit assumption that each microbiome

sample must belong to a *single* signature “community” characterized by the cluster centroid. As some authors note [Holmes et al. \[2012\]](#), [Mao et al. \[2020\]](#), this assumption is often unrealistic and overly restrictive for complex environments such as the gut microbiome. Several recent developments embrace the more relaxed biological hypothesis that the ASVs characterizing a microbiota sample hail from a combination of multiple microbial “clusters”, or more precisely “subcommunities”.

Mixed-membership (MM) models are a generalization of clustering models which allow samples to have fractional membership in clusters and so provide a generative modeling framework for data involving subcommunity structures [Deek and Li \[2019\]](#), [Sankaran and Holmes \[2019\]](#), [Shafei et al. \[2015\]](#). In modeling microbiome compositions, MM models allow each microbiome sample to be composed of multiple microbial subcommunities. Sankaran and Holmes [Sankaran and Holmes \[2019\]](#) applied the most well-known MM model, the latent Dirichlet allocation (LDA) model, to microbiome profiling, while Shafei et al [Shafei et al. \[2015\]](#) and Deek and Li [Deek and Li \[2019\]](#) proposed variations of LDA accounting for environmental factors and inflated zero-counts, respectively.

The key motivation for our paper is the observation that existing MM models such as LDA — originally developed in other contexts such as topic modeling and population genetics — do not incorporate several key features of microbiome sequencing data. Most notably, they assume that a microbiome subcommunity must be *exactly the same* in terms of the composition of the involved microbes for all samples. This is a highly unrealistic assumption in the vast majority of microbiome studies where the samples often display high levels of heterogeneity. It is interesting to note that such heterogeneity has been well-recognized in clustering models for microbiome data [Holmes et al. \[2012\]](#), [Mao et al. \[2020\]](#), but has been largely ignored in existing application of MM models.

Additionally, in other common applications of MM models, such as in topic modelling, it is an almost ubiquitous practice to overspecify the number of “topics”—corresponding to the subcommunities in the current context—in the hope that some meaningful subcommunities will emerge amongst many others. We will demonstrate that without accounting for cross-sample heterogeneity this practice can be not only counterproductive but also misleading in the microbiome context.

We introduce a generalization to the LDA model that aims to appropriately incorporate

“random effects”, i.e., cross-sample heterogeneity in microbiomal subcommunity compositions due to unmeasured sources, thereby leading to more accurate identification of subcommunities in MM models. Our approach takes advantage of the availability of a natural tree structure relating the microbial taxa—the phylogenetic tree—which allows us to decompose the compositional vector into a collection of binomial observations, one for each of the tree nodes. This transform serves two purposes. First, it allows us to model the heterogeneity by modeling the vector of log-odds transforms of the binomial probabilities at each node as a latent multivariate Gaussian. By modeling the subcommunity compositions as realizations from this logistic-tree normal (LTN) [Wang et al. \[2021\]](#) distribution, we are able to impose appropriate constraints on the underlying covariance structure to ensure the identifiability of the subcommunities. A second purpose of the tree-based transform is computational. We show that under this transform, by utilizing the so-called Pólya-Gamma (PG) data augmentation technique [Polson et al. \[2013\]](#), inference under the resulting MM model can be readily accomplished through fully conjugate collapsed blocked Gibbs sampling. We term our new model logistic-tree normal latent Dirichlet allocation (LTN-LDA).

In the following, we will briefly review the LDA and LTN models before introducing the LTN-LDA model. We will derive the posterior for the LTN-LDA model using a class of auxiliary Pólya-Gamma variables [Polson et al. \[2013\]](#) and present a collapsed blocked Gibbs sampler for carrying out Bayesian inference. We will demonstrate in simulations that the inference produced by LTN-LDA is robust with respect to overspecifying the number of subcommunities while inference under LDA can be highly sensitive to such overspecifications in the presence of cross-sample heterogeneity. We will then apply LTN-LDA to the dataset of [Dethlefsen and Relman \[2011\]](#).

2 Methods

2.1 Latent Dirichlet Allocation

Let there be D samples consisting of counts of V unique ASVs indexed by $1, 2, \dots, V$. For sample d , let $\mathbf{x}_d = (x_{d,1}, \dots, x_{d,V})$ be the vector of ASV counts such that $x_{d,v}$ is the total count for ASV v in sample d . Let $N_d = \sum_{v=1}^V x_{d,v}$ be the sum of counts in sample d , which

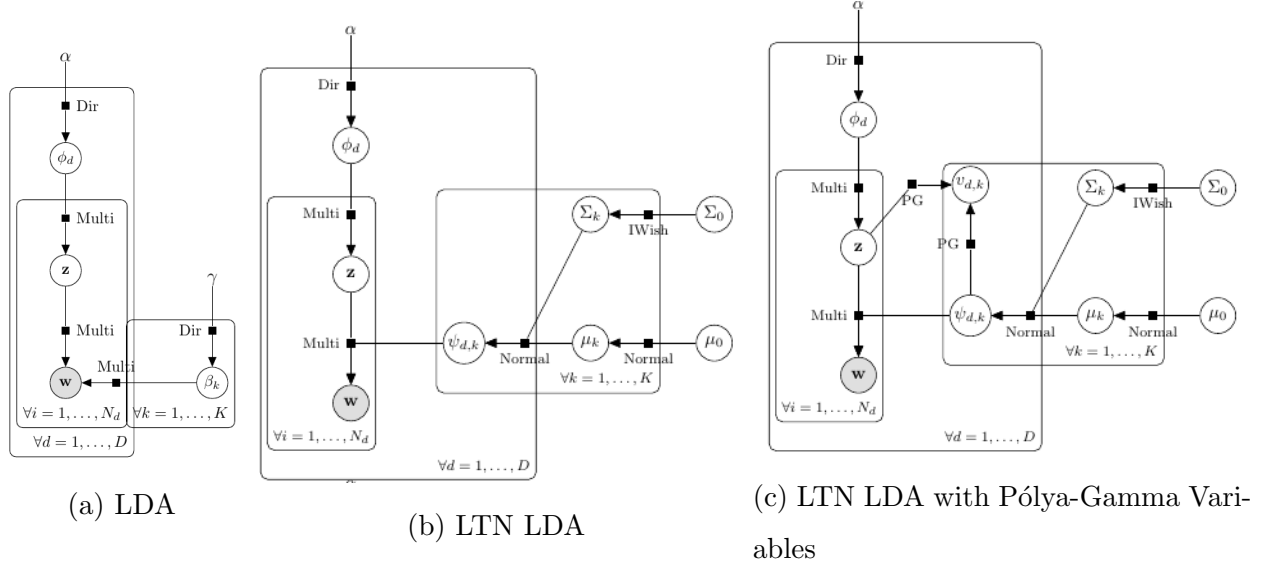


Figure 1: Graphical model representations for LDA and LTN-LDA.

is determined by the sequencing depth.

Subcommunities are defined to be collections of ASVs that co-occur in samples at given relative proportions. The composition of a subcommunity is the relative proportions of the corresponding ASVs within that subcommunity. An ASV can occur in multiple subcommunities at various abundances and the key assumption underlying an MM model, in contrast to a clustering model, is that different instances (i.e., the sequencing read counts) of the same ASV in a sample can potentially be resulting from the presence of multiple subcommunities. Key parameters of interest in MM models are the proportions of the various subcommunities in each sample, which we refer to as the subcommunity abundance, along with the subcommunity composition—the proportions of the ASVs involved—of each subcommunity.

To describe MM models, it is convenient to introduce multinomial-Bernoulli indicators for each read count and its associated subcommunity identity. To this end, for $d = 1, 2, \dots, D$, let \mathbf{w}_d be a vector $\mathbf{w}_d = (w_{d,1}, \dots, w_{d,N_d})$ where $w_{d,n} \in \{1, 2, \dots, V\}$ is multinomial-Bernoulli indicator of the ASV associated with the n th read count in the sample. We refer to the elements $w_{d,n}$ in this vector as “tokens” to draw analogy with other contexts in which MM models are applied. In particular, in topic modelling, each token is a word in a document; here, each token corresponds to a read count associated with an ASV. We also note that $x_{d,v} = \sum_{n=1}^{N_d} \mathbf{1}_{\{w_{d,n}=v\}}$.

Let $\boldsymbol{\phi}_d = (\phi_d^1, \phi_d^2, \dots, \phi_d^K)'$ in the K -dimensional simplex be the subcommunity abundance vector. That is, ϕ_d^k represent the relative abundance of subcommunity k in sample d , and so $\boldsymbol{\phi}_d$ specifies the multinomial-Bernoulli distribution of each token over the K underlying subcommunities in sample d . Let $z_{d,n}$ represent the subcommunity from which the n^{th} token in sample d arises from and let \mathbf{z} be the vector all such assignments for sample d . Also, let $\boldsymbol{\beta}_k = (\beta_k^1, \beta_k^2, \dots, \beta_k^V)'$ be the subcommunity composition for subcommunity k . That is, $\boldsymbol{\beta}_k$ lies in the V -dimensional simplex and gives the relative proportions of the V unique ASVs in subcommunity k . The LDA model Blei et al. [2003] in the current context then becomes

$$\begin{aligned} w_{d,n}|z_{d,n}, \boldsymbol{\beta}_{z_{d,n}} &\sim Mult(1, \boldsymbol{\beta}_{z_{d,n}}) \text{ for } d = 1, \dots, D \text{ and } n = 1, \dots, N_d \\ z_{d,n}|\boldsymbol{\phi}_d &\sim Mult(1, \boldsymbol{\phi}_d) \text{ for } d = 1, \dots, D \\ \boldsymbol{\phi}_d|\alpha &\sim Dir(\alpha) \text{ for } d = 1, \dots, D \\ \boldsymbol{\beta}_k|\gamma &\sim Dir(\gamma) \text{ for } k = 1, \dots, K, \end{aligned}$$

and the graphical model is presented in Figure 1a.

Though LDA can be applied in the microbiome context Sankaran and Holmes [2019], it does not account for the cross-sample heterogeneity in the distribution of ASVs per subcommunity. In particular, it assumes that the distributions of ASVs-per-subcommunity, $\boldsymbol{\beta}_k$, are the *exact same* across all samples. This assumption is inconsistent with the empirical behavior of the microbiome setting where large cross-sample heterogeneities exist Mao et al. [2020]. We will demonstrate that this has two main effects: LDA interprets cross-sample heterogeneity as the presence of additional subcommunities and thus overestimates the “true” number of subcommunities, and inference provided by the LDA model can change radically as the number of subcommunities changes.

2.2 Incorporating cross-sample heterogeneity

We shall enrich the LDA framework to allow cross-sample heterogeneity in the subcommunity compositions. There are several widely used hierarchical models for microbiome compositions in the literature such as the Dirichlet-Multinomial (DM) model Holmes et al. [2012], Nigam et al. [2000] and Aitchinson’s log-ratio based normal (LN) models Aitchison [1982], all of which could in principle be embedded into the LDA for this purpose. However, the DM is highly restrictive in its ability to characterize the underlying cross-sample variability as

the Dirichlet distribution has only a single scalar variance parameter, while the LN models are computationally challenging due to the lack of conjugacy to the multinomial sampling model. To resolve these difficulties, we adopt the recently introduced logistic-tree normal (LTN) model Wang et al. [2021] to obtain both modeling flexibility and computational efficiency. In particular, we will show that the LTN model can be readily embedded into the LDA model to accommodate cross-sample heterogeneity and that posterior inference can be readily accomplished through simple collapsed blocked Gibbs sampling using a data-augmentation technique called the Pólya-Gamma augmentation. Moreover, we note that, since the adoption of the LTN model requires specifying a dyadic partition tree on the ASVs, the phylogenetic tree relating the taxa is the natural tree structure to use. In the following, we briefly introduce the phylogenetic tree and the LTN model constructed based on the phylogenetic tree, before embedding the LTN model into LDA to form our new mixed-membership model.

2.2.1 The Phylogenetic Tree

Let \mathcal{T} denote a phylogenetic tree encapsulating the evolutionary relationships among the observed ASVs. The leaf nodes in the tree correspond to the observed ASVs in the data set. Each interior node is the inferred common ancestral taxon for the ASVs lying in the corresponding descendant subtree at the node. Each node (or taxon) A in the phylogenetic tree \mathcal{T} can be represented by the collection of its descendant ASVs. In particular, each leaf node A contains a single ASV, whereas each internal node A contains multiple ASVs. In the following, we let \mathcal{L} be the set of leaf nodes of \mathcal{T} , and \mathcal{I} the internal nodes. Throughout this work, we shall assume that the phylogenetic tree is binary, in the sense that each interior node A has exactly two child nodes (i.e., direct descendants).

An example tree is included in Fig. 2. For this tree, the internal nodes are labeled $\{7, 8, \dots, 11\}$, and the leaf nodes are labeled $1, 2, \dots, 6$. The interior node 8 for example, is the set of two ASVs associated with nodes 1 and 2, while the root, node 7, corresponds to the set of all 6 ASVs represented by the leaves.

For each node $A \in \mathcal{I}$ we let A_l and A_r be the left and right children of A , respectively. For each node $A \in \mathcal{T}$, we use $y(A)$ to denote the total sequencing read counts associated with all ASVs or leaves descended from A . When there are multiple subcommunities and samples,

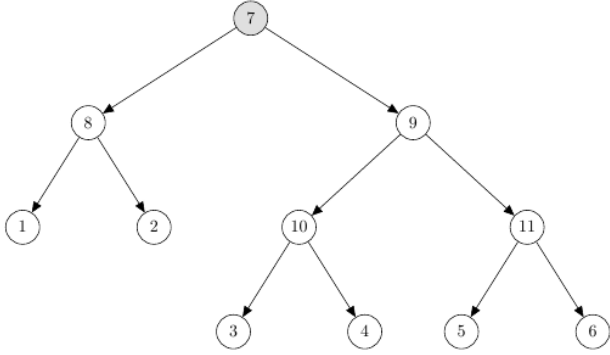


Figure 2: An Example Tree

we extend this notation to $y_{d,k}(A)$ which is the total sequencing read counts associated with all ASVs or leaves descended from A in subcommunity k and sample d .

2.2.2 The LTN Model

The LTN model is based on a factorization of the multinomial distribution of ASVs on the leaves of \mathcal{T} for subcommunity k and sample d , $\boldsymbol{\beta}_{d,k} = (\beta_{d,k}^1, \beta_{d,k}^2, \dots, \beta_{d,k}^V)'$, into a set of binomial distributions on the internal nodes \mathcal{I} . For each internal node $A \in \mathcal{I}$, for each subcommunity k , and for each sample d , we define

$$\theta_{d,k}(A) = \frac{\sum_{v \in A_l} \beta_{d,k}^v}{\sum_{v \in A} \beta_{d,k}^v},$$

which expresses the probability that a token descended from A is also descended from A_l under $\boldsymbol{\beta}_{d,k}$. The binomial likelihood at each node is thus

$$y_{d,k}(A_l) | y_{d,k}(A), \theta_{d,k}(A) \sim \text{Binomial}(y_{d,k}(A_l) | y_{d,k}(A), \theta_{d,k}(A)).$$

Let $\boldsymbol{\theta}_{d,k}$ be a vector containing the values of $\theta_{d,k}(A)$ with respect to an ordering on the $p = |\mathcal{I}|$ internal nodes of \mathcal{T} and note that $\boldsymbol{\theta}_{d,k}$ is in one-to-one correspondence with $\boldsymbol{\beta}_{d,k}$.

Let $\psi_{d,k}(A) = \log \frac{\theta_{d,k}(A)}{1 - \theta_{d,k}(A)}$ be the log-odds transform of $\theta_{d,k}(A)$ and let $\boldsymbol{\psi}_{d,k}$ be the vector of $\psi_{d,k}(A)$ with respect to the same ordering on the p internal nodes of \mathcal{T} . Then for each d we model

$$\boldsymbol{\psi}_{d,k} | \boldsymbol{\mu}_k, \Sigma_k \sim N(\boldsymbol{\mu}_k, \Sigma_k),$$

for some mean vector $\boldsymbol{\mu}_k$ and covariance matrix Σ_k associated with subcommunity k . We

place conjugate priors on $\boldsymbol{\mu}_k$ and Σ_k , giving rise to a hierarchical LTN model:

$$\begin{aligned}
y_{d,k}(A_l) | \psi_{d,k}(A) &\sim \text{Bin}(y_{d,k}(A), \theta_{d,k}(A)) \text{ for } d = 1, \dots, D, k = 1, \dots, K \text{ and, } A \in \mathcal{I} \\
\psi_{d,k} | \boldsymbol{\mu}_k, \Sigma_k &\sim N(\boldsymbol{\mu}_k, \Sigma_k) \\
\boldsymbol{\mu}_k &\sim N(\boldsymbol{\mu}_0, \Lambda_0) \\
\Sigma_k &\sim F,
\end{aligned}$$

where F is some prior distribution on Σ .

2.3 Logistic-Tree Normal Latent Dirichlet Allocation

We incorporate the LTN model into LDA to allow cross-sample heterogeneity in subcommunity compositions. The resulting model is termed logistic-tree normal latent Dirichlet allocation (LTN-LDA).

Let $y_{d,k}(A)$ represent the count of all sequencing reads descended from node A in sample d assigned to subcommunity k . Let $\psi_{d,k}(A) \in \mathbb{R}$ represent the log-odds at node A in sample d in subcommunity k . Let $\boldsymbol{\psi}_{d,k}$ be the vector of $\psi_{d,k}(A)$ for each d and k . Let $\boldsymbol{\mu}_k$ be the vector of average log-odds in subcommunity k , and let Σ_k be the associated covariance matrix. If there are N_d ASVs in the d^{th} sample then the generative model is

$$\begin{aligned}
y_{d,k}(A_l) | \psi_{d,k}(A) &\sim \text{Bin}(y_{d,k}(A), \theta_{d,k}(A)) \text{ for } d = 1, \dots, D, k = 1, \dots, K, \text{ and, } A \in \mathcal{I} \\
z_{d,n} | \boldsymbol{\phi}_d &\stackrel{\text{iid}}{\sim} \text{Mult}(1, \boldsymbol{\phi}_d) \text{ for } d = 1, \dots, D \text{ and } n = 1, \dots, N_d \\
\boldsymbol{\phi}_d &\stackrel{\text{iid}}{\sim} \text{Dir}(\alpha) \text{ for } d = 1, \dots, D \\
\boldsymbol{\psi}_{d,k} | \boldsymbol{\mu}_k, \Sigma_k &\stackrel{\text{iid}}{\sim} \text{MVN}(\boldsymbol{\mu}_k, \Sigma_k), \text{ for } d = 1, \dots, D, k = 1, \dots, K \\
\boldsymbol{\mu}_k &\stackrel{\text{iid}}{\sim} \text{MVN}(\boldsymbol{\mu}_0, \Lambda_0) \\
\Sigma_k &\stackrel{\text{iid}}{\sim} F.
\end{aligned}$$

Here μ_0 and Λ_0 are given. The graphical model is in Fig 1b.

The key distinction between LTN-LDA and LDA is that LTN-LDA uses an LTN to model the varying compositions of each subcommunity across the samples. In particular, the composition of subcommunity k in sample d is determined by $\boldsymbol{\psi}_{d,k}$, which is allowed to vary across d .

Without additional assumptions or constraints on the high-dimensional covariance matrices for each subcommunity, Σ_k , the model is generally too flexible, tends to overfit the data, and can even become unidentifiable at typical sample sizes for microbiome studies. Additional structural constraints on the covariance structure are thus necessary. We adopt the additional structural constraint that Σ_k is a diagonal covariance matrix. While the assumption may appear overly strong, we note that the dependence among the tree-based log-odds ratios are generally weak in stark contrast to the often very strong and complex dependence structure among the ASV counts themselves. In a sense, the tree-based log-odd transform of the abundance vectors “decorrelates” the data.

Aside from the diagonal covariance assumption, we also enforce that the amount of variability for each node depends on that node’s distance to the bottom (i.e., leaf) level of the tree. In particular, we assume that taxa close to the bottom of the phylogenetic tree have larger cross-sample variability in the corresponding log-odds ratio than those which are distant. This is consistent with empirical observations, as well as the biological intuition that taxa which are deep in the tree tend to have comparable functionality. Their relative proportions thus often display elevated levels of variance due to their functional exchangeability.

Specifically, let $|A|$ encapsulate the distance of A from the leaf level by denoting the number of leaves descended from node A . The prior on Σ_k we adopt has the form

$$\begin{aligned}\Sigma_k &= \text{diag}(\tau_{i,k}) \text{ for } i = 1, \dots, p \text{ and } k = 1, \dots, K \\ \tau_{i,k} &\propto \text{IG}(a_1, b) \text{ if } |A_i| \geq C \\ \tau_{i,k} &\propto \text{IG}(a_2, b) \text{ if } |A_i| < C\end{aligned}$$

for $C \in \mathbb{N}$ which may be treated as a tuning parameter. This choice of priors ensures conjugate updating, avoids the identifiability problem, and allows cross-sample heterogeneity in biologically justifiable manner. We can choose a_1 , a_2 , and b in such a manner that nodes high in the tree have low expected variance in the posterior, while nodes low in the tree have a high expectation.

2.4 Bayesian Inference by Collapsed Blocked Gibbs Sampling

2.4.1 Pólya-Gamma Latent Variables

The LTN-LDA model presented thus far is not conjugate; to make it so we introduce Pólya-Gamma latent variables [Polson et al. \[2013\]](#).

We rewrite the binomial likelihood at each internal node A as

$$\begin{aligned} \text{Bin}(y_{d,k}(A_l)|y_{d,k}(A), \psi_{d,k}(A)) &\propto \frac{(e^{\psi_{d,k}(A)})^{y_{d,k}(A_l)}}{(1 + e^{\psi_{d,k}(A)})^{y_{d,k}(A)}} \\ &= 2^{-y_{d,k}(A)} e^{\kappa_{d,k}(A)\psi_{d,k}(A)} \int_0^\infty e^{-v_{d,k}(A)\psi_{d,k}(A)^2} p(v_{d,k}(A)) dv_{d,k}(A), \end{aligned}$$

where $\kappa_{d,k}(A) = y_{d,k}(A_l) - \frac{y_{d,k}(A)}{2}$ and

$$p(v_{d,k}(A)) = \frac{2^{y_{d,k}(A)-1}}{\Gamma(y_{d,k}(A))} \sum_{n=0}^{\infty} (-1)^n \frac{n + y_{d,k}(A)}{n+1} \frac{(2n + y_{d,k}(A))}{\sqrt{2\pi v_{d,k}(A)^3}} \exp\left[-\frac{(2n + y_{d,k}(A))^2}{8v_{d,k}(A)}\right],$$

is the probability density function of a $PG(y_{d,k}(A), 0)$ distribution. We thus introduce a class of latent variables $v_{d,k}(A)$ independent of $y_{d,k}(A_l)$ conditioned on $y_{d,k}(A)$ and $\psi_{d,k}(A)$:

$$v_{d,k}(A)|y_{d,k}(A), \psi_{d,k}(A) \sim PG(y_{d,k}(A), \psi_{d,k}(A)).$$

The marginal likelihood of $y_{d,k}(A_l)$ conditioned on $v_{d,k}(A)$ is then

$$\exp\left((y_{d,k}(A_l) - \frac{y_{d,k}(A)}{2})\psi_{d,k}(A) - \frac{v_{d,k}(A)\psi_{d,k}(A)^2}{2}\right),$$

which is conjugate with the multivariate Gaussian likelihood of $\psi_{d,k}$. The graphical model for LTN-LDA with the Pólya-Gamma variables is presented in Figure 1c.

For notational purposes let $\mathbf{v}_{d,k}$ be the vector of $v_{d,k}(A)$ and let $\boldsymbol{\kappa}_{d,k}$ be the vector of $\kappa_{d,k}(A)$.

2.4.2 Collapsed Blocked Gibbs Sampler

We integrate the ϕ_d out of the sampling model and proceed with a collapsed Gibbs sampler to improve convergence [Griffiths and Steyvers \[2004\]](#). The full conditionals we will sample from are thus

- (1) $(\mathbf{v}_{d,k}, \mathbf{z}_d) \sim p(v_{d,k}(A), \mathbf{z}_d | \boldsymbol{\psi}_{d,k}, \boldsymbol{\mu}_k, \Sigma_k)$
- (2) $\psi_{d,k} \sim p(\boldsymbol{\psi}_{d,k} | \mathbf{v}_{d,k}, \mathbf{z}_d, \boldsymbol{\mu}_k, \Sigma_k)$
- (3) $\boldsymbol{\mu}_k \sim p(\boldsymbol{\mu}_k | \mathbf{v}_{d,k}, \mathbf{z}_d, \boldsymbol{\psi}_{d,k}, \Sigma_k)$
- (4) $\Sigma_k \sim p(\Sigma_k | \mathbf{v}_{d,k}, \mathbf{z}_d, \boldsymbol{\psi}, \boldsymbol{\mu}_k),$

The joint full conditional $(v_{d,k}(A), \mathbf{z}_d)$ is

$$\begin{aligned}\mathbf{z}_d &\sim p(\mathbf{z}_d | \psi_{d,k}, \boldsymbol{\mu}_k, \Sigma_k) \\ v_{d,k}(A) &\sim p(v_{d,k}(A) | \mathbf{z}_d, \psi_{d,k}(A), \boldsymbol{\mu}_k, \Sigma_k).\end{aligned}$$

To sample the vector \mathbf{z}_d from its full conditional, we sample each subcommunity assignment in order from its multinomial full conditional:

$$p(z_{d,n} = k | \mathbf{z}_d^{-n}, \psi_{d,k}(A), \boldsymbol{\mu}_k, \Sigma_k) \propto (y_{d,k}(\mathcal{R})^{-n} + \alpha) \times \beta_k^{w_{d,n}},$$

where \mathbf{z}_d^{-n} is the vector of all subcommunity assignments in sample d except for $z_{d,n}$ and $y_{d,k}(\mathcal{R})^{-n}$ is the number of sequencing reads in sample d descended from the root node \mathcal{R} assigned to subcommunity k not counting the n^{th} token. Note that we can estimate the value of $\boldsymbol{\phi}_d$ from the \mathbf{z}_d by

$$\hat{\boldsymbol{\phi}}_d = \frac{1}{\sum_{k=1}^K y_{d,k}(\mathcal{R}) + K\alpha} \begin{bmatrix} y_{d,1}(\mathcal{R}) + \alpha & \dots & y_{d,K}(\mathcal{R}) + \alpha \end{bmatrix}$$

The full conditional for $v_{d,k}(A)$ is

$$v_{d,k}(A) | y_{d,k}(A), \psi_{d,k}(A) \sim PG(y_{d,k}(A), \psi_{d,k}(A)),$$

the full conditional of a Pólya-Gamma distribution derived in [Polson et al. \[2013\]](#). However, existing Pólya-Gamma samplers are slow and so for large values of $y_{d,k}(A)$ we use an approximate Pólya-Gamma sampler proposed in [Glynn et al. \[2019\]](#). In this case,

$$p(v_{d,k}(A) | \mathbf{z}_d) \approx N \left[\frac{y_{d,k}(A)^2}{2\psi_{d,k}(A)} \tanh \left(\frac{\psi_{d,k}(A)}{2} \right), \frac{y_{d,k}(A)^2}{4\psi_{d,k}(A)^3} \operatorname{sech}^2 \left(\frac{\psi_{d,k}(A)}{2} \right) (\sinh(\psi_{d,k}(A)) - \psi_{d,k}(A)) \right]$$

The full conditionals for $\boldsymbol{\mu}_k$ and $\tau_{i,k}$ follow by conjugate updating:

$$\begin{aligned}\boldsymbol{\mu}_k &\sim MVN((\Lambda^{-1} + D\Sigma^{-1})^{-1} \Sigma_k^{-1} D \bar{\boldsymbol{\psi}}_{D,k}, (\Lambda^{-1} + D\Sigma_k^{-1})^{-1}) \\ \tau_{i,k} &\sim IG(a_1 + \frac{D}{2}, \frac{2b + \sum_{d=1}^D (\psi_{d,k}(A_i) - \mu_k(A_i))^2}{2}) \quad \text{if } |A_i| \geq C \\ \tau_{i,k} &\sim IG(a_2 + \frac{D}{2}, \frac{2b + \sum_{d=1}^D (\psi_{d,k}(A_i) - \mu_k(A_i))^2}{2}) \quad \text{if } |A_i| < C\end{aligned}$$

Further, the full conditional for $\boldsymbol{\psi}_{d,k}$ is also multivariate normal,

$$\boldsymbol{\psi}_{d,k} \sim MVN((\Sigma^{-1} + \operatorname{diag}(\mathbf{v}_{d,k}))^{-1} (\Sigma^{-1} \boldsymbol{\mu} + \boldsymbol{\kappa}_{d,k}), (\Sigma^{-1} + \operatorname{diag}(\mathbf{v}_{d,k}))^{-1}),$$

by [Polson et al. \[2013\]](#).

3 Numerical experiments

3.1 Robustness in choosing the number of subcommunities

A common strategy in application of MM models in contexts such as topic modeling is to overspecify K and hoping that a subset of identified subcommunities will correspond to contextually meaningful ones because the true number of subcommunities K in a given data set is typically unknown. However, for data with large cross-sample heterogeneity such as microbiome compositions, intuition suggests that a model that does not allow such heterogeneity will confuse sample-specific variations around a subcommunity mean with the presence of additional subcommunities, resulting in inference which is highly sensitive to the choice of K .

To verify this intuition, we first generate data from a true known LTN-LDA model which allows cross-sample heterogeneity. In particular, we simulate $D = 50$ samples and $N_d = 10,000$ sequencing reads per sample, while the various hyperparameters are $\alpha = 1$, $\mu = 0$, $\Lambda = I$, $a_1 = 10^4$, and $a_2 = b = 10$. We set the true number of subcommunities to be $K = 4$ and the cutoff point to be $C = 10$. The underlying phylogenetic tree used is presented in Figure 3: there are 49 leaves and 48 internal nodes, and each color indicates a region where the majority — approximately 77.5 percent — of the total abundance of a subcommunity is located.

We now contrast LDA and LTN-LDA by running collapsed blocked Gibbs samplers on the data generated above with $K \in \{4, 5, 7, 10\}$. For now we set the modelled value of C in the LTN-LDA sampler equal to 10, the truth. In the next subsection we will examine strategies for setting the tuning parameters C and K . In the left part of Figure 4, we plot the posterior means of the subcommunity abundances ϕ_d for both LDA and LTN-LDA. For each value of K , LDA subcommunities are matched to LTN-LDA subcommunities to minimize the L_2 distances between the β_k distributions.

With K set to the true value, LDA performs comparably to LTN-LDA in terms of estimating the true values of ϕ_d . However, as we increase K beyond the true value, the inference provided by LDA worsens. While it can still roughly estimate the correct abundances for subcommunities 1 and 2, it fails to do so for subcommunities 3 and 4. At the same time, LDA detects the presence of additional subcommunities which do not exist in the true generative

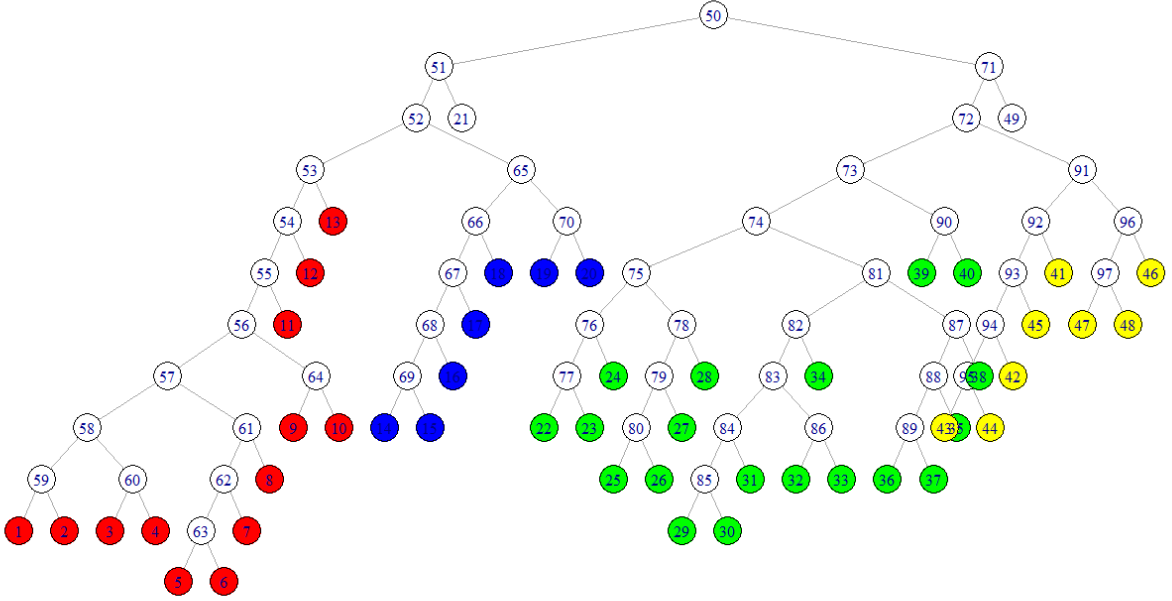


Figure 3: The phylogenetic tree used in simulations

model. LTN-LDA, in contrast, is remarkably stable when the K is overspecified: no matter the modelled value of K , it detects the four true subcommunities with approximately the same abundances. Additional subcommunities have very little estimated abundance.

For $K = 10$, we plotted the ASV-subcommunity distributions on the right part of Figure 4. Distributions for the $\beta_{d,k}$ are in blue and the β_k are in red for LTN-LDA; the LDA β_k distributions are in black. LTN-LDA finds some moderate levels of cross-sample heterogeneity in subcommunity 2, and a high levels in samples 3 and 4.

These two figures imply that LDA is able to recover the subcommunity abundances only for those subcommunities with low levels of cross-sample heterogeneity. LDA fails to recover the subcommunity abundances for those subcommunities with high levels of cross-sample heterogeneity; it instead mistakes cross-sample heterogeneity as additional subcommunities. LTN-LDA, on the other hand, provides stable and accurate inference as the modelled value of K increases. Thus, if we were to adopt an approach of overestimating the number subcommunities in our model with the hope of recovering meaningful subcommunities in the presence of cross-sample heterogeneity, we will be misled if we use LDA but not if we use LTN-LDA.

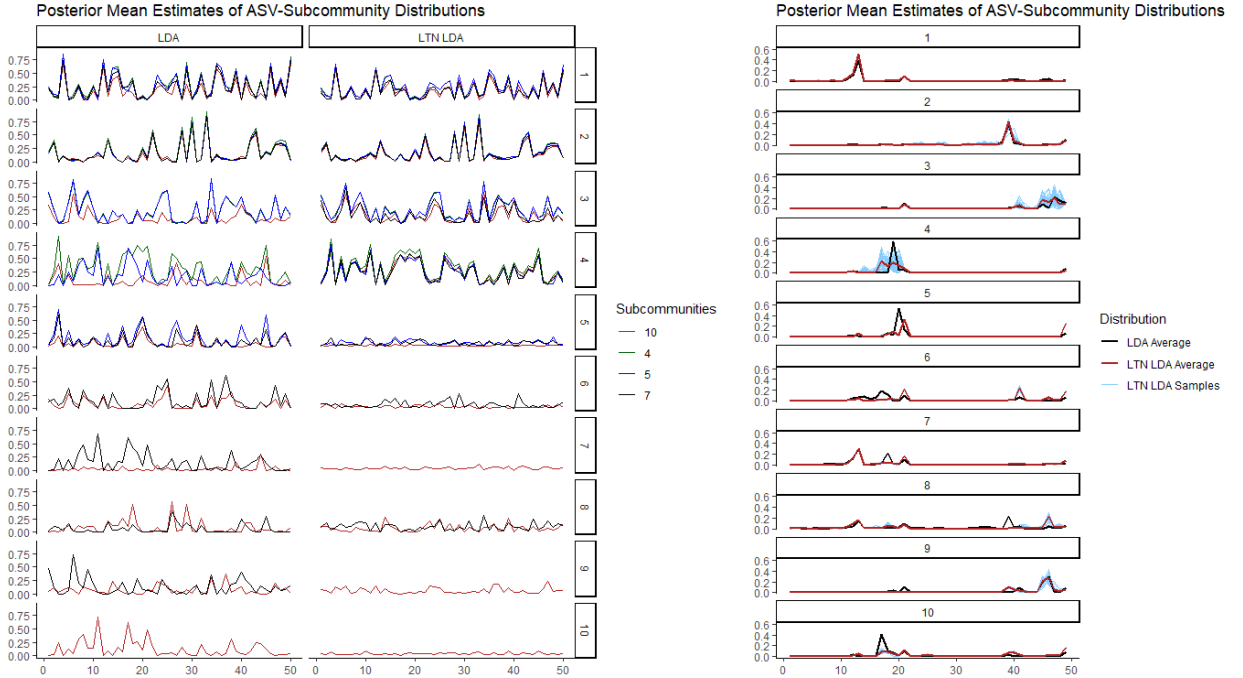


Figure 4: (Left) Subcommunity abundance for ϕ_d for all samples over four different numbers of subcommunities $K \in \{4, 5, 7, 10\}$ for LDA (left) and LTN-LDA (right). The estimated abundances are noticeably more stable over different values of K for the LTN-LDA. (Right) Estimated subcommunity compositions for all samples. Blue indicates the sample-specific composition under LTN-LDA ($\beta_{d,k}$, red indicates the average subcommunity composition under LTN-LDA (β_k) and black indicates the average subcommunity composition (β_k) under LDA. The 49 ASVs are on the x-axis.

3.2 Predictive scoring as a device for choosing tuning parameters

While incorporating cross-sample heterogeneity enhances the robustness of LTN-LDA to overspecifying the number of subcommunities, it is still useful to have a generally applicable strategy for setting the tuning parameters for LTN-LDA: K and C . To this end, one can use out-of-sample predictive performance to identify suitable choices of the tuning parameters. A popular performance measure for MM models — originally designed for LDA in the topic modeling context — is perplexity, which is a transform of out-of-sample predictive score such that lower perplexity scores indicate better out-of-sample performance.

We thus examine the simple strategy of computing the average out-of-sample perplexity score for different choices of (K, C) and examine whether that can lead to a practical way of choosing these parameters. We will also examine whether this strategy could be adopted for models without cross-sample heterogeneity, namely LDA, to eliminate, or at least alleviate, their limitation. We follow the procedure proposed in Section 5.1 of [Wallach et al. \[2009\]](#) for computing the perplexity for LDA, and generalize that strategy to computing the perplexity score for LTN-LDA. We defer the technical details on the perplexity and the procedures for computing to [Supplement A](#) for the interested reader.

We generate 200 simulated datasets. In each, there are $D = 50$ samples and $N_d = 10,000$ sequencing reads per sample, while the various hyperparameters values are set to $\alpha = 1$, $\mu = 0$, $\Lambda = I$, $a_1 = 10^4$, and $a_2 = b = 10$. The true value of K is 4 and the true value of C is 10. For each dataset, we also generate a test set of 50 samples with 10,000 sequencing reads per sample. We use $\alpha = 1$ to generate the ϕ_d and use the same μ_k and Σ_k as the training set to generate the $\psi_{d,k}$.

First, fixing the modelled value of C to its true value (which we will later relax), we computed average perplexity results across the 200 datasets for LDA and LTN-LDA as we varied the number of modelled subcommunities K in [Figure 5a](#). There are three main points: (a) LTN-LDA significantly outperforms LDA for K near truth, (b) the perplexity curve for LTN-LDA decreases until it stabilizes at the true value of K , (c) the perplexity curve for LDA continues to decrease if the modelled K is increased past its true value.

We believe that the main reason that the two models behave so differently is that LDA interprets the presence of cross-sample heterogeneity as extra subcommunities and will find

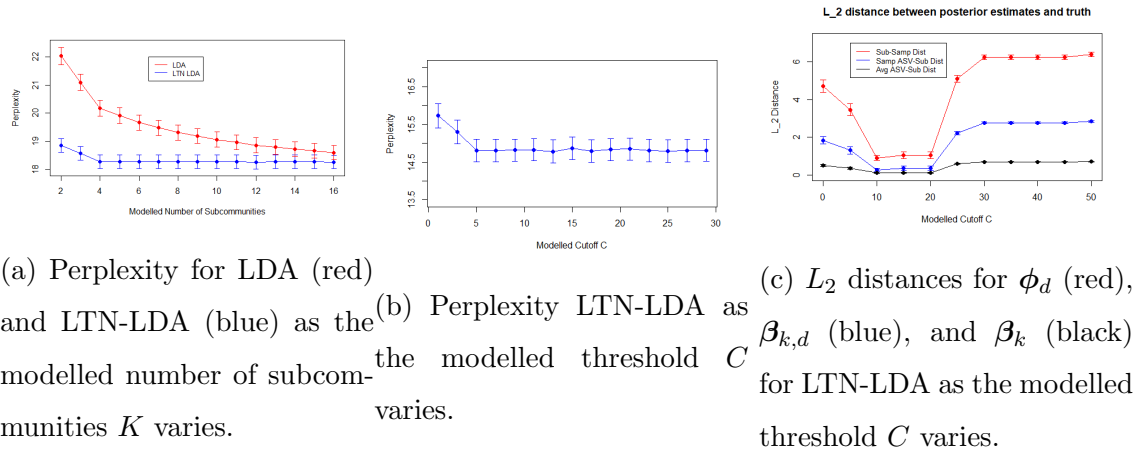


Figure 5: Simulation Results

as many subcommunities as are modelled. This improves out of sample predictive performance even though it does not improve inference to the truth. Thus, using perplexity to select the modelled number of subcommunities for LDA is a poor method in the presence of significant cross-sample heterogeneity. On the other hand, by incorporating cross-sample heterogeneity in subcommunity compositions, LTN-LDA is more robust and parsimonious in its representation of the data.

Fixing the modelled value of K to its true value, we computed average perplexity results across the 200 datasets for LTN-LDA as we varied the modelled threshold C in Figure 5b. Note that LTN-LDA with a threshold $C = 0$ is similar to LDA as it allows only very small levels of cross-sample heterogeneity and so may be taken as a point of comparison. The perplexity curve shows the same behavior as it did above: it decreases until it stabilizes at the true value of C .

For the same datasets, we computed the L_2 distances between posterior mean estimates and true values for the ϕ_d , $\beta_{d,k}$, and β_k distributions (Figure 5c). The L_2 distances allow us to assess how close posterior estimates are to truth. Unlike the perplexity curves, which stabilize after reaching the true value of C , the L_2 distances are lowest around the true true cutoff point $C = 10$. Thus, if the modelled value of C is increased too far above its true value, inference to the truth worsens. This suggests that choosing C is an important step in modelling: if it is too low or too high, inference to truth will be poor.

The above results suggest a simple two-stage strategy for choosing tuning parameters for

LTN-LDA based on perplexity. In the first stage, one can let K and C vary jointly on a grid and use either a test set or cross-validation to compute the average perplexity. This results in K perplexity curves over C . Set the value of C to be the inflection point in these curves. Then in the second stage, one can vary K and set the value of K to be the inflection point of the resulting perplexity curve. Note that this strategy will not generally work for LDA, as our numerical examples show that due to the lack of cross-sample heterogeneity in LDA, the perplexity score generally continues to improve as one increase the number of subcommunities way beyond the true number of subcommunities. This in turn will lead to misleading inference on the subcommunity abundance and composition as we showed in the previous section.

4 Evaluation on a microbiome study

We apply LTN-LDA to identify subcommunity dynamics in the dataset of Dethlefsen and Relman [Dethlefsen and Relman \[2011\]](#), which has been previously investigated by other authors using LDA [Sankaran and Holmes \[2019\]](#). The data includes the gut microbiome composition of three patients who were administered two five day courses of ciprofloxacin over a ten month span. For ease of comparison, we follow [Sankaran and Holmes \[2019\]](#) and focus on the 54 samples from patient F — each of approximately 10,000 ASVs — which were collected at uneven intervals. The antibiotic regimens were given in two intervals for samples 12 through 23 and samples 41 through 51 respectively.

There are 2,852 unique ASVs in dataset used in [Sankaran and Holmes \[2019\]](#) and publicly available on Kris Sankaran’s gitbhub. We merged ASVs into taxa at their finest known taxa and pruned all taxa which total at least 100 sequencing reads across all 54 samples. This left 44 taxa totalling 99.86 percent of the original counts. The resulting phylogenetic tree is presented in Figure 6.

We implemented the strategy outlined above to choose tuning parameters. In particular, we implement a 4-fold cross-validation in setting K based on perplexity where K is allowed to vary in $\{2, 3, \dots, 8\}$ and C is allowed to vary in $\{1, 2, \dots, 21\}$. The resulting K perplexity curves over C are presented in Figure 7a. The inflection point in the curve appears at $C = 8$ and so we choose this value for C . Varying the modelled K gives the results in

Figure 7b. In comparison, we also applied LDA to the data over varying K . LTN-LDA has strictly lower perplexity than LDA does across all modelled values of K , indicating that there is significant levels of cross-sample heterogeneity in the dataset. Moreover, LTN-LDA experiences a noticeable inflection point (near 5) in contrast to LDA whose perplexity decays slowly over a much wider range of K values.

We now present more detailed analysis for LTN-LDA and LDA with $C = 8$. For $K \in \{3, 4, 7\}$ we plotted the subcommunity abundance on the left side of Figure 8. The grey regions indicate time periods when patient F underwent antibiotic treatment. For each K , we matched LDA subcommunities to LTN-LDA subcommunities by finding the subcommunity permutation which minimized L_2 between the β_k distributions for LDA and LTN-LDA.

The subcommunities found by LTN-LDA are remarkably stable as K changes: subcommunities 1, 2, and 3 have almost the exact same abundance. Moreover, when additional subcommunities are added, LTN-LDA finds that they have minimal abundance. LDA, however, finds as many subcommunities as are modelled. Further, LDA subcommunities are not stable as K varies — there is not a single subcommunity which has the same sample prevalence for all three values of K .

For $K = 7$, we plotted the ASV-subcommunity distributions on the right side of Figure 8. Distributions for the $\beta_{d,k}$ are in blue and the β_k are in red, while the LDA distributions are in black. The 5 most prevalent ASVs in each subcommunity are presented in Figure 9 for both LDA and LTN-LDA. These two plots demonstrate that LTN-LDA finds significant levels of cross-sample heterogeneity and provides meaningfully different subcommunity compositions than LDA.

We now analyze the three stable subcommunities found by LTN-LDA. The first subcommunity, which falls off dramatically during periods of antibiotic treatment and recovers otherwise, is composed mostly of Lachnospiraceae and Ruminococcaceae. The second subcommunity is composed mainly of Bacteroides and saw an increase in relative abundance during the antibiotic treatments: this may indicate that it simply is more antibiotic-resistant than the first subcommunity. Both of these phenomena have been observed in mice [Zhu et al. \[2020\]](#) and humans [Stewardson et al. \[2015\]](#). The third subcommunity is much less prevalent, spiking only at the first day of the second antibiotic course, but it is persistent as K changes. It is composed mostly of Dialister and Veillonella. Ciprofloxacin has been shown to be effective

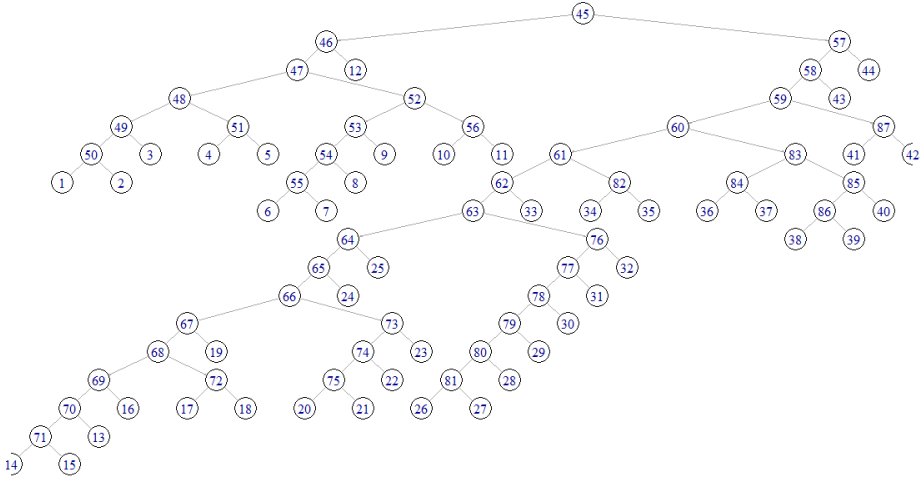


Figure 6: The phylogenetic tree for the Dethlefsen and Relman data after merging and pruning

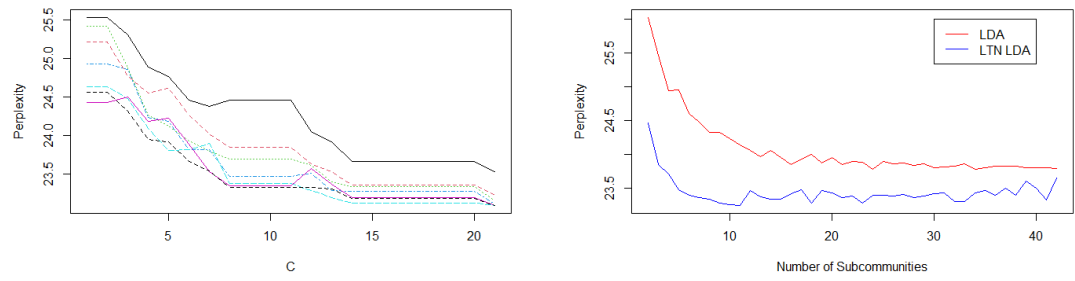
against Dialister Morio et al. [2007] which may explain the decrease in this subcommunity after treatment began.

5 Discussion

We have proposed a novel mixed-membership model which seeks to appropriately incorporate cross-sample heterogeneity in subcommunity compositions: a characteristic of the data prevalent in most microbiome studies. By incorporating a logistic-tree normal model for the sample-specific compositions of each subcommunity, we explicitly allow the composition of subcommunities to vary across samples.

We have shown that incorporating cross-sample heterogeneity into MM models can lead to substantially improved inference. In particular, the popular strategy of overspecifying the number of subcommunities is only reasonable when such heterogeneity is accounted for. As such, LTN-LDA is substantially more robust than LDA with respect to such overspecifications.

LTN-LDA also significantly outperforms LDA in terms of predictive performance as mea-



(a) Perplexity for varying levels on K on the Dethlefsen and Relman data as we vary $C = 8$.
(b) Perplexity for LTN LDA and LDA as K varies while $C = 8$.

Figure 7: Cross-validation results

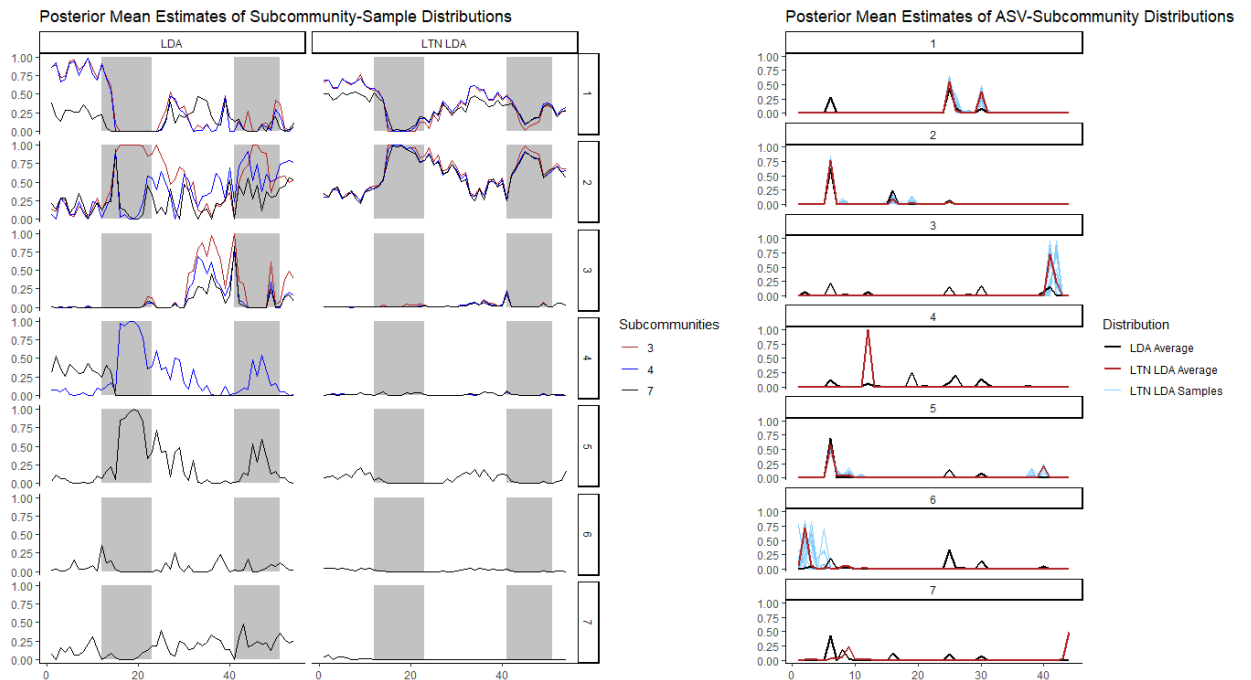


Figure 8: (Left) Subcommunity abundance for ϕ_d for all samples over three different numbers of subcommunities $K \in \{3, 4, 7\}$ for LDA (left) and LTN-LDA (right). The estimated abundances are noticeably more stable over different values of K for the LTN-LDA. (Right) Estimated subcommunity compositions for all samples. Blue indicates the sample-specific composition under LTN-LDA ($\beta_{k,d}$), red indicates the average subcommunity composition under LTN-LDA (β_k) and black indicates the average subcommunity composition (β_k) under LDA. The 44 ASVs are on the x-axis.

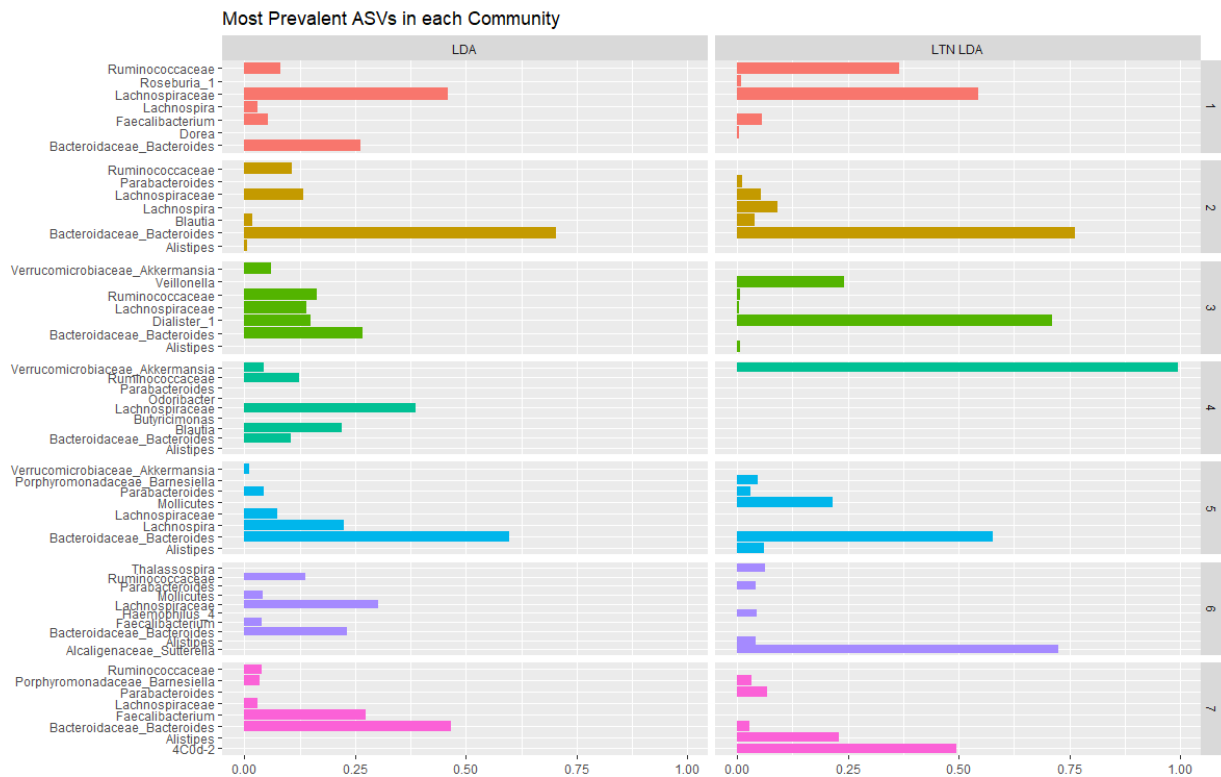


Figure 9: The 5 most prevalent ASVs in each subcommunity for LDA and LTN LDA, $K = 7$, $C = 8$.

sured by perplexity in the presence of cross-sample heterogeneity. Moreover, in the microbiome context, predictive score can be a useful device to set the tuning parameters for LTN-LDA but not for LDA due to the cross-sample heterogeneity. Posterior computation on the LTN-LDA can proceed through collapsed blocked Gibbs-sampling with the assistance of Pólya-Gamma augmentation, and as such implementation for LTN-LDA is convenient.

We believe that the idea of incorporating cross-sample heterogeneity in MM models could be valuable beyond the context of microbiome compositions. In topic models, for example, one might expect different authors to write on the same topic using different vocabulary. LTN-LDA has the potential to be applicable to these other contexts as well, though the immediate challenge which must be overcome is finding an appropriate tree structure.

6 Software

Reproducible code and data will be available shortly at <https://github.com/PatrickLeBlanc/ReproduceLTNLDAPaper>. R code for implementing the LTN-LDA model is available in the LTNLDA package <https://github.com/PatrickLeBlanc/LTNLDA>.

Acknowledgment

This research is supported by NIGMS grant R01-GM135440. Part of the research was completed when PL was supported by an IBIEM fellowship at Duke University.

References

John Aitchison. The statistical analysis of compositional data. *Journal of the Royal Statistical Society. Series B (Methodological)*, 44(2):139–177, 1982.

Francesco Beghini, Lauren J McIver, Aitor Blanco-Míguez, Leonard Dubois, Francesco Asnicar, Sagun Maharjan, Ana Mailyan, Paolo Manghi, Matthias Scholz, Andrew Maltez Thomas, Mireia Valles-Colomer, George Weingart, Yancong Zhang, Moreno Zolfo, Curtis Huttenhower, Eric A Franzosa, and Nicola Segata. Integrating taxonomic, functional, and strain-level profiling of diverse microbial communities with biobakery 3. *Elife*, 2021.

David M. Blei, Andrew Y. Ng, and Michael I. Jordan. Latent dirichlet allocation. *Journal of Machine Learning Research*, 3:993–1022, 2003.

Benjamin J Callahan, Paul J McMurdie, and Susan P Holmes. Exact sequence variants should replace operational taxonomic units in marker-gene data analysis. *The ISME Journal*, 11:2639–2643, 2017.

Paul I. Costea, Falk Hildebrand, Manimozhiyan Arumugam, Fredrik Backhed, Martin J. Blaser, Frederic D. Bushman, Willem M. de Vos, S. Dusko Ehrlich, Claire M. Fraser, Masahira Hattori, Curtis Huttenhower, Ian B. Jeffery, Dan Knights, James D. Lewis, Ruth E. Ley, Howard Ochman, Paul W. O’Toole, Christopher Quince, David A. Relman, Fergus Shanahan, Shinichi Sunagawa, Jun Wang, George M. Weinstock, Gary D. Wu, Georg Zeller, Liping Zhao, Jeroen Raes, Rob Knight, and Peer Bork. Enterotypes in the landscape of gut microbial community composition. *Nature Microbiology*, 3:8–16, 2018.

Rebecca A Deek and Hongzhe Li. A zero-inflated latent dirichlet allocation model for microbiome studies. *Frontiers in Genetics*, 11:599–614, 2019.

Federica Del Chierico, Pamela Vernocchi, Bruno Dallapiccola, and Lorenza Putignani. Mediterranean diet and health: Food effects on gut microbiota and disease control. *International Journal of Molecular Sciences*, 15(7):11678–11699, 2014.

Les Dethlefsen and David A. Relman. Incomplete recovery and individualized responses of the human distal gut microbiota to repeated antibiotic perturbation. *Proceedings of the National Academy of the Sciences of the United States of America*, 108(Supplement 1):4554–4561, 2011.

Chris Glynn, Surya T. Tokdar, Brian Howard, and David L. Banks. Bayesian Analysis of Dynamic Linear Topic Models. *Bayesian Analysis*, 14(1):53 – 80, 2019.

Thomas L. Griffiths and Mark Steyvers. Finding scientific topics. *Proceedings of the National Academy of Sciences*, 101(suppl 1):5228–5235, 2004.

Ian Holmes, Keith Harris, and Christopher Quince. Dirichlet multinomial mixtures: Generative models for microbial metagenomics. *PLoS ONE*, 7(2), 2012.

Hongzhe Li. Microbiome, metagenomics, and high-dimensional compositional data analysis. *Annual Review of Statistics and Its Application*, 2(1):73–94, 2015.

Jialiang Mao, Yuhua Chen, and Li Ma. Bayesian graphical compositional regression for microbiome data. *Journal of the American Statistical Association*, 115(530):610–624, 2020.

F. Morio, H. Jean-Pierre, L. Dubreuil, E. Jumas-Bilak, L. Calvet, G. Mercier, R. Devine, and H. Marchandin. Antimicrobial susceptibilities and clinical sources of dialister species. *Antimicrobial Agents and Chemotherapy*, 51(12):4498–4501, 2007.

Kamal Nigam, Andrew Kachites Mccallum, Sebastian Thrun, and Tom Mitchell. Text classification from labeled and unlabeled documents using em. *Machine Learning*, 39:103–134, 2000.

Nicholas G. Polson, James G. Scott, and Jesse Windle. Bayesian inference for logistic models using polya–gamma latent variables. *Journal of the American Statistical Association*, 108(504):1339–1349, 2013.

Kris Sankaran and Susan P Holmes. Latent variable modeling for the microbiome. *Biostatistics*, 20(4):599–614, 2019.

Mahdi Shafiei, Katherine A Dunn, Eva Boon, Shelley M MacDonald, David A Walsh, Hong Gu, and Joseph P Bielawski. Biomico: a supervised bayesian model for inference of microbial community structure. *Microbiome*, 3(8), 2015.

A.J. Stewardson, N. Gaia, P. Francois, S. Malhotra-Kumar, C. Delemont, B. Martinez de Tejada, J. Schrenzel, S. Harbarth, and V. Lazarevic. Collateral damage from oral ciprofloxacin versus nitrofurantoin in outpatients with urinary tract infections: a culture-free analysis of gut microbiota. *Clinical Microbiology and Infection*, 21(4):344.e1–344.e11, 2015.

Yunfan Tang, Li Ma, and Dan L. Nicolae. A phylogenetic scan test on a Dirichlet-tree multinomial model for microbiome data. *The Annals of Applied Statistics*, 12(1):1–26, 2018.

Hanna M. Wallach, Iain Murray, Ruslan Salakhutdinov, and David Mimno. Evaluation methods for topic models. *Proceedings of the 26th Annual International Conference on Machine Learning*, page 1105–1112, 2009.

Tao Wang and Hongyu Zhao. A dirichlet-tree multinomial regression model for associating dietary nutrients with gut microorganisms. *Biometrics*, 73(3):792–801, 2017.

Zhuoqun Wang, Jialiang Mao, and Li Ma. Logistic-tree normal model for microbiome compositions, 2021.

Shengyun Zhu, Huiqi Li, Jing Liang, Chaoran Lv, Kai Zhao, Mingshan Niu, Zhenyu Li, Lingyu Zeng, and Kailin Xu. Assessment of oral ciprofloxacin impaired gut barrier integrity on gut bacteria in mice. *International Immunopharmacology*, 83, 2020.

Supplement A: Perplexity

Perplexity is a metric of predictive performance which is commonly used for mixed-membership models in a topic modelling setting, but which can be adapted to the microbiome context. It is a transform of the predictive likelihood on a test set. Let $d = 1, \dots, D_{te}$ be samples in a test set, each of length N_d , and let \mathcal{M} be the collection of parameters specifying a model. The perplexity for model \mathcal{M} is defined as

$$\exp \left(- \frac{\sum_{d=1}^{D_{te}} \log p(\mathbf{w}_d | \mathcal{M})}{\sum_{d=1}^{D_{te}} N_d} \right).$$

A lower perplexity value implies a higher out-of-sample predictive likelihood and is thus desired.

Wallach et al. [2009] describes procedures for computing perplexity for LDA. We modify the document-completion procedure detailed in section 5.1 for LTN-LDA. First, we fit the model on a training set, and recover posterior mean estimates for the μ_k and Σ_k .

Every sample in the test set, d^{te} , is randomly divided in two halves with approximately equal sequencing counts and ASV distributions: $d^{te,(1)}$ and $d^{te,(2)}$. It suffices to consider only one sample, d . We run a modified version of the collapsed blocked Gibbs sampler for LTN-LDA on $d^{te,(1)}$ with the values of μ_k and Σ_k fixed at the posterior mean estimates found in the training set. This enables us to estimate the sample-specific parameters ϕ_d , \mathbf{z}_d , and $\psi_{d,k}$ in $d^{te,(1)}$.

The perplexity is found using $d^{te,(2)}$ as follows. Let $\mathbf{w}_d^{te,(1)}$ and $\mathbf{w}_d^{te,(2)}$ be the vectors of sequencing reads in $d^{te,(1)}$ and $d^{te,(2)}$ respectively. Let $\phi_{d,k}^{te,(1)}(i)$ and $\beta_{d,k,v}^{te,(1)}(i)$ be the values of ϕ_d^k and $\beta_{k,d}^v$ found in $d^{te,(1)}$ at iteration i . Then we can estimate $p(\mathbf{w}_d^{te,(2)} | \mathbf{w}_d^{te,(1)}, \mathcal{M}) = p(\mathbf{w}_d^{te,(2)} | \mathbf{w}_d^{te,(1)}, \boldsymbol{\beta}_{k,d}^{te,(1)}, \boldsymbol{\phi}_d^{te,(1)})$. We average over iterations to obtain a Monte Carlo estimate of the log-likelihood:

$$\log p(\mathbf{w}_{d,n}^{te,(2)} | \phi_{d,k}^{te,(1)}(i), \beta_{k,d,w_{d,n}^{te,(2)}}^{te,(1)}(i)) \approx \frac{1}{I} \sum_{i=1}^I \sum_n \log \left(\sum_{k=1}^K \phi_{d,k}^{te,(1)}(i) \beta_{k,d,w_{d,n}^{te,(2)}}^{te,(1)}(i) \right),$$

which can be transformed into an estimated perplexity value for the sample.